

**FINITE DIFFERENCE TIME DOMAIN MODELING OF INFRASOUND PROPAGATION:  
APPLICATION TO SHADOW ZONE ARRIVALS AND REGIONAL PROPAGATION**

Catherine de Groot-Hedlin

University of California at San Diego

Sponsored by Army Space and Missile Defense Command

Contract No. W9113M-06-1-0003

Proposal No. BAA06-95

**ABSTRACT**

The finite difference (FD) method yields solutions to discretized versions of the full acoustic wave equation for arbitrarily complex media. The method is reliable at all angles of propagation, including backscatter. This offers an advantage over other standard propagation methods in wide use, as it allows for accurate computation of acoustic energy levels in the case where significant scattering can occur near the source, such as may happen for an explosion near the surface, or underground. It also allows for the investigation of the penetration of infrasound energy into classical shadow zones, where ray theory predicts the upward refraction of sound. This fits in with nuclear monitoring goals, in that it allows for an improved understanding of the generation and propagation of infrasound energy from arbitrary sources, including underground and near-surface explosions.

The effects of 1) wind, 2) attenuation, and 3) gravity on infrasound propagation are examined separately, using finite-difference time-domain methods. The method is applied in 2-D Cartesian coordinates. The method, including the effects of wind, is applied to realistic problems in infrasound propagation, including the penetration of infrasound energy into “shadow” zones, as defined by ray theory. The effects of diffraction and topography are examined for sources near the surface. It is shown that the FD approach can be used to solve for sound intensities in complex models that may include high material contrasts and arbitrary topography.

| Report Documentation Page  |                                    |                                     |   | Form Approved<br>OMB No. 0704-0188                  |                                 |
|--|------------------------------------|-------------------------------------|---|---|---------------------------------|
| Public reporting burden for the collection of information is estimated to average 1 hour per response, including the time for reviewing instructions, searching existing data sources, gathering and maintaining the data needed, and completing and reviewing the collection of information. Send comments regarding this burden estimate or any other aspect of this collection of information, including suggestions for reducing this burden, to Washington Headquarters Services, Directorate for Information Operations and Reports, 1215 Jefferson Davis Highway, Suite 1204, Arlington VA 22202-4302. Respondents should be aware that notwithstanding any other provision of law, no person shall be subject to a penalty for failing to comply with a collection of information if it does not display a currently valid OMB control number. |                                    |                                     |   |   |                                 |
| 1. REPORT DATE<br><b>SEP 2008</b>  |                                    | 2. REPORT TYPE                      |   | 3. DATES COVERED<br><b>00-00-2008 to 00-00-2008</b> |                                 |
| 4. TITLE AND SUBTITLE<br><b>Finite Difference Time Domain Modeling of Infrasound Propagation: Application to Shadow Zone Arrivals and Regional Propagation</b>   |                                    |                                     |   | 5a. CONTRACT NUMBER                                 |                                 |
|  |                                    |                                     |   | 5b. GRANT NUMBER                                    |                                 |
|  |                                    |                                     |   | 5c. PROGRAM ELEMENT NUMBER                          |                                 |
| 6. AUTHOR(S)   |                                    |                                     |   | 5d. PROJECT NUMBER                                  |                                 |
|  |                                    |                                     |   | 5e. TASK NUMBER                                     |                                 |
|  |                                    |                                     |   | 5f. WORK UNIT NUMBER                                |                                 |
| 7. PERFORMING ORGANIZATION NAME(S) AND ADDRESS(ES)<br><b>University of California at San Diego, 9500 Gilman Dr, La Jolla, CA, 92093</b>  |                                    |                                     |   | 8. PERFORMING ORGANIZATION REPORT NUMBER            |                                 |
| 9. SPONSORING/MONITORING AGENCY NAME(S) AND ADDRESS(ES)  |                                    |                                     |   | 10. SPONSOR/MONITOR'S ACRONYM(S)                    |                                 |
|  |                                    |                                     |   | 11. SPONSOR/MONITOR'S REPORT NUMBER(S)              |                                 |
| 12. DISTRIBUTION/AVAILABILITY STATEMENT<br><b>Approved for public release; distribution unlimited</b>  |                                    |                                     |   |   |                                 |
| 13. SUPPLEMENTARY NOTES<br><b>Proceedings of the 30th Monitoring Research Review: Ground-Based Nuclear Explosion Monitoring Technologies, 23-25 Sep 2008, Portsmouth, VA sponsored by the National Nuclear Security Administration (NNSA) and the Air Force Research Laboratory (AFRL)</b>   |                                    |                                     |   |   |                                 |
| 14. ABSTRACT<br><b>see report</b>  |                                    |                                     |   |   |                                 |
| 15. SUBJECT TERMS  |                                    |                                     |   |   |                                 |
| 16. SECURITY CLASSIFICATION OF:  |                                    |                                     | 17. LIMITATION OF ABSTRACT<br><b>Same as Report (SAR)</b> | 18. NUMBER OF PAGES<br><b>10</b>                    | 19a. NAME OF RESPONSIBLE PERSON |
| a. REPORT<br><b>unclassified</b>   | b. ABSTRACT<br><b>unclassified</b> | c. THIS PAGE<br><b>unclassified</b> |   |   |                                 |

## **OBJECTIVES**

A finite difference time domain (FDTD) method is sought for the numerical propagation of infrasound energy through realistic atmosphere properties, including variable winds, sound speeds, and density variations, and the interaction of the sound field with topography. The FDTD method yields the solution to a discretized version of the full acoustic wave equation for arbitrarily complex media, and can accurately handle propagation reliable at all angles of propagation, including backscatter. This offers an advantage over other standard propagation methods in wide use, as it allows for an accurate computation in cases where significant scattering can occur near the source, such as may happen for an explosion near the surface or underground. The effects of wind or gravity on infrasound propagation may also be incorporated into the infrasound propagation problem with relative ease using FD techniques. In this paper, a method to handle the inclusion of attenuation into the time-domain computations is investigated, as well as the effects of topography on infrasound.

The equation governing the effects of gravity, wind, and attenuation on the infrasound field are derived in this paper, and their effects on propagation through the atmosphere are demonstrated. The penetration of infrasound into a classical “shadow zone” is also demonstrated both for a model of a source above a flat surface with high impedance contrast, and also for the same source, above a rough surface with high impedance contrast. In this way, we examine the effects of topography on propagation of infrasound energy into a shadow zone.

## **RESEARCH ACCOMPLISHED**

Equations governing infrasound propagation through the atmosphere are derived here. The effects of gravity, wind, and atmospheric attenuation of the acoustic field are examined separately. Following that, the effects of topography on infrasound penetration into an acoustic shadow zone are shown. In each case, the methods are applied in 2-D Cartesian coordinates.

### ***Linear acoustic propagation equations***

The equations governing propagation of sound in the atmosphere are

i) the conservation of momentum,

$$\rho \frac{D\vec{v}}{Dt} = -\nabla p + \vec{F}, \quad (1)$$

which relates the particle velocity,  $\vec{v}$ , to the total pressure,  $p$ , and density,  $\rho$ , and the external volume force per unit mass,  $\vec{F}$ ;

ii) the conservation of mass,

$$\frac{D\rho}{Dt} = -\rho \nabla \cdot \vec{v}, \quad (2)$$

iii) and the equation of state,

$$\frac{Dp}{Dt} = c^2 \frac{D\rho}{Dt}, \quad (3)$$

where  $c$  is the total sound speed in the presence of acoustic perturbations. It's assumed in the equation above that infrasound propagation is isentropic, i.e., that entropy is constant. That is, it's assumed that attenuation is sufficiently small so that wave propagation dominates over diffusive propagation. This is a valid approximation for infrasound propagation within a realistic atmosphere.

The convective derivative (also known as the Lagrangian derivative) acting on a quantity  $G$  is defined as

$$\frac{DG}{Dt} = \frac{\partial G}{\partial t} + (\vec{v} \cdot \nabla)G, \quad (4)$$

where the derivative on the left represents the change of  $G$  with time in a frame moving with the fluid. The first term on the right side of Equation 4 represents the change in  $G$  at a point fixed in space. The second term, called the advective term, represents the change in  $G$  as the observer moves with the fluid at the velocity  $\vec{v}$ . For infrasound investigations, quantities are expressed in terms of a fixed point in space in order to compare computational results with observations made at stationary sensors.

Propagation of sound waves in the atmosphere introduces fluctuations in the pressure, density, and particle velocity values. The standard procedure in solving Eqs. 1 through 3 is to consider a perturbed solution of the form

$$p = p_o + p_s; \quad \rho = \rho_o + \rho_s; \quad \vec{v} = \vec{v}_o + \vec{v}_s, \quad c^2 = c_o^2 + c_s^2; \quad (5)$$

where  $p_o$ ,  $\rho_o$ , and  $\vec{v}_o$  are the ambient values of pressure, density, and particle velocity in the absence of perturbations, and  $p_s$ ,  $\rho_s$ , and  $\vec{v}_s$  are perturbations caused by the passage of a sound wave. The pressure fluctuations cause slight fluctuations in the squared sound speed. Waveforms are derived by computing the pressure perturbations,  $p_s$ , as a function of time. Linear expressions for the particle velocity,  $\vec{v}_s$ , and pressure and density fluctuations,  $p_s$  and  $\rho_s$ , are derived by retaining only first order terms in the pressure, velocity, and density. The zeroth order terms cancel because the ambient atmosphere is assumed to be in equilibrium.

### *Linearized acoustic propagation, including gravitational effects*

In this sub-section, we consider solutions in a static medium, thus  $\vec{v}_o$ , denoting the wind velocity, is equal to zero. If the effects of gravity are included in the propagation equations, the external volume force per unit mass may be expressed as

$$\vec{F} = -(\rho_o + \rho_s)\vec{g} + \vec{f}, \quad (6)$$

where the gravity  $\vec{g} = [0, 0, 9.8 \text{ m/s}^2]$ , and  $\vec{f}$  represents all external forces other than gravity. Using Eqs. 5 and 6 in Eq. 1, and linearizing, yields

$$\rho_o \frac{\partial \vec{v}_s}{\partial t} = -\nabla p_s - \rho_s \vec{g} + \vec{f}. \quad (7)$$

under the assumption that there is no wind, and using the hydrostatic equation  $\nabla p_o = -\rho_o \vec{g}$ . Combining Eqs. 2 and 3 yields the following expression for pressure perturbations

$$\frac{\partial p_s}{\partial t} = \rho_o \vec{v}_s \cdot \vec{g} - \rho_o c_o^2 \nabla \cdot \vec{v}_s, \quad (8)$$

where the hydrostatic equation has again been used. Horizontal gradients in the ambient pressure and density,  $p_o$  and  $\rho_o$ , are negligible in the horizontal direction. Equation 2 becomes

$$\frac{\partial \rho_s}{\partial t} + \vec{v}_s \cdot \nabla \rho_o = \frac{1}{c_o^2} \left[ \frac{\partial p_s}{\partial t} + \vec{v}_s \cdot \nabla p_o \right]. \quad (9)$$

Combining the ideal gas law ( $p_o = \rho_o RT$ ) with the hydrostatic equation, and the relation between sound speed and temperature ( $c_o^2 = \gamma RT$ ) yields

$$\frac{d\rho_o}{dz} = -\frac{\gamma \rho_o g}{c_o^2} - \frac{2\rho_o}{c_o} \frac{dc}{dz}, \quad (10)$$

where  $\gamma \approx 1.402$ ,  $T$  is the temperature in degrees Kelvin and  $R$  is the gas constant for dry air,  $R = 287.04 \text{ J kg}^{-1} \text{ K}^{-1}$ . Using the hydrostatic equation for vertical pressure gradients and Eq. 10 for vertical density gradients, Eq. 9 can be expressed as

$$\frac{\partial \rho_s}{\partial t} = \frac{1}{c_o^2} \frac{\partial p_s}{\partial t} + \rho_o \vec{v}_s \cdot \left[ \frac{(\gamma - 1)\vec{g}}{c_o^2} + \frac{2}{c_o} \nabla c_o \right]. \quad (11)$$

Equations 7, 8, and 11 are a complete set of equations, in a form amenable to FD time domain computations.

Note that Eq. 11 may also be expressed as (Gill, 1982)

$$\frac{\partial \rho_s}{\partial t} - \rho_o \vec{v}_s N^2 / \vec{g} = \frac{1}{c_o^2} \frac{\partial p_s}{\partial t}, \quad (12)$$

where the Brunt-Vaisala frequency  $N$ —or buoyancy frequency—is defined by

$$N^2 = g_z \left( \frac{(\gamma - 1)g_z}{c_o^2} + \frac{2}{c_o} \nabla c_o \right). \quad (13)$$

The buoyancy frequency  $N$  is on the order of  $1/300$  Hz within the atmosphere. The equations suggest that the effect of buoyancy is negligible at the upper end of the infrasound range but becomes more significant with decreasing frequency. Results of computations are compared below for sources with peak frequencies of 0.2 Hz and 0.015 Hz, for  $g_z = 0$  and  $g_z = 9.8 \text{ m/s}^2$ . In each case the sound speeds are assumed to be uniform (i.e., an isothermal atmosphere) and exponentially decreasing density. The results confirm that gravitational effects are insignificant at higher frequency.

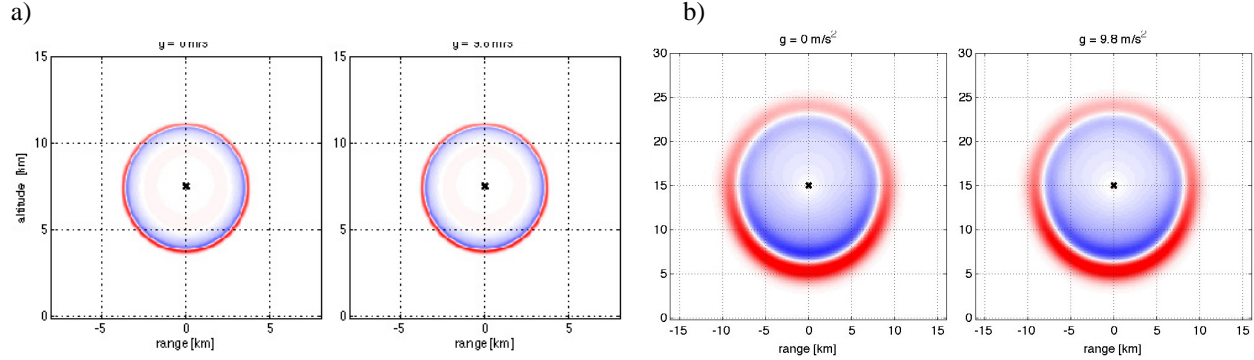


**Figure 1. Results shown above are for models with exponentially decreasing density. a) The source peak frequency is 0.2 Hz. There is less than 0.2% difference between the solution for  $g=0$  and for  $g=9.8 \text{ m/s}^2$ . B) The case for a source peak frequency of 0.015 Hz. There is less than 3.5% difference between the solution for  $g=0$  and for  $g=9.8 \text{ m/s}^2$ .**

#### Linearized acoustic propagation, including wind and gravitational effects

When wind is included, i.e.,  $\bar{v}_O \neq 0$ , we use Eq. 4, the convective derivative to find

$$\rho_O \left( \frac{\partial \bar{v}_S}{\partial t} + \bar{v}_S \cdot \nabla \bar{v}_O + \bar{v}_O \cdot \nabla \bar{v}_S \right) + \rho_S \bar{v}_O \cdot \nabla \bar{v}_O = -\nabla p_S - \rho_S \bar{g} + \bar{f}, \quad (14)$$

for particle velocity. Re-arranging, and assuming that wind is invariant along path ( $\bar{v}_O \cdot \nabla \bar{v}_O = 0$ , which is true for negligible turbulence) this becomes

$$\frac{\partial \bar{v}_S}{\partial t} = -\bar{v}_S \cdot \nabla \bar{v}_O - \bar{v}_O \cdot \nabla \bar{v}_S - \frac{1}{\rho_O} (\nabla p_S + \rho_S \bar{g} - \bar{f}), \quad (15)$$

i.e. wind shear is included in this formulation. The above result differs from Ostashev et.al. (2005) in that gravity is included and thus density perturbations must be computed.

The equation for pressure perturbations becomes

$$\frac{\partial p_S}{\partial t} + \bar{v}_S \cdot \nabla p_O + \bar{v}_O \cdot \nabla p_S = -\rho_O c_O^2 \nabla \cdot \bar{v}_S - \rho_O c_S^2 \nabla \cdot \bar{v}_O - \rho_S c_O^2 \nabla \cdot \bar{v}_O \quad (16)$$

It's assumed that turbulence is insignificant (as in Ostashev et.al., 2005) so  $\nabla \cdot \bar{v}_O$  is negligible. The hydrostatic equation is used to get the following form for pressure perturbations:

$$\frac{\partial p_S}{\partial t} = \rho_O \bar{v}_S \cdot \bar{g} - \bar{v}_O \cdot \nabla p_S - \rho_O c_O^2 \nabla \cdot \bar{v}_S \quad (17)$$

The equation for density perturbations becomes

$$c_O^2 \left[ \frac{\partial \rho_S}{\partial t} + \bar{v}_S \cdot \nabla \rho_O + \bar{v}_O \cdot \nabla \rho_S \right] + c_S^2 (\bar{v}_O \cdot \nabla \rho_O) = \frac{\partial p_S}{\partial t} + \bar{v}_S \cdot \nabla p_O + \bar{v}_O \cdot \nabla p_S \quad (18)$$

Winds are horizontal and the ambient density varies only with altitude, so  $\bar{v}_O \cdot \nabla \rho_O = 0$ . So, using the hydrostatic equation for  $\nabla p_O$  and Equation 10 for the spatial density derivative  $\nabla \rho_O$  and rearranging yields

$$\frac{\partial \rho_s}{\partial t} = \frac{1}{c_o^2} \left[ \frac{\partial p_s}{\partial t} + \bar{v}_O \cdot \nabla p_s \right] + \rho_O \bar{v}_s \cdot \left[ \frac{(\gamma - 1) \bar{g}}{c_o^2} + \frac{2}{c_o} \nabla c_o \right] - \bar{v}_O \cdot \nabla \rho_s \quad (19)$$

Equations 15, 17, and 19 are a complete set of equations for the propagation of infrasound energy, including gravity and wind, in a form amenable to FDTD implementation.

An example showing the sound field for realistic sound, wind, and density profiles (Figure 2a) is shown in Figure 2b, for a source at 100 km altitude, with a center frequency of 0.1 Hz. Densities and temperature profile data for a location near the I57US infrasound station were derived from the MSIS-90 atmospheric model, made available through <http://nssdc.gsfc.nasa.gov/space/model/models/msis.html>. Wind data were derived from the Horizontal Wind Model (HWM) 1993 program (Hedin et.al., 1996). The results shown in Figure 3 are for the pressure field at 108 sec after the "explosion." As indicated, the pressure field is asymmetric due to the effects of wind, although the Mach numbers for this example are less than  $M=0.15$  at all altitudes. The pressure field is shown in the panel at left, the pressure field normalized by  $\rho_o^{-1/2}$  is shown in the panel at right. As indicated, the scaled pressure field is reasonably uniform with this scaling.

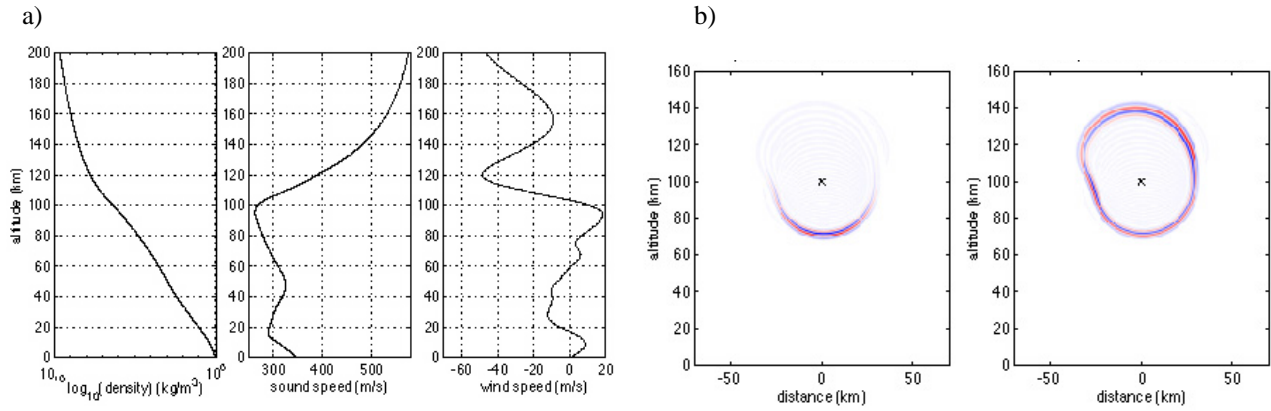


**Figure 2. a) Profiles for atmospheric density, sound speed, and wind speed. b) Pressure field (left) and the pressure field scaled by  $\rho_o^{-1/2}$  (right) for a source with center frequency at 0.1 Hz and at an altitude of 100 km, for medium properties, as shown in Figure 2a.**

#### *Linearized acoustic propagation, including attenuation, wind and gravitational effects*

It has been shown that atmospheric attenuation is approximately proportional to the square of frequency (Sutherland and Bass, 2004; de Groot-Hedlin, 2008a). It can be shown (Batchelor, 1967), that the effects of atmospheric attenuation can be included by adding two terms to the equation for conservation of

momentum:  $\mu(\nabla^2 \bar{v}_s + \frac{1}{3} \nabla(\nabla \cdot \bar{v}_s))$ , where  $\nabla^2 \bar{v}_s$  is a vector with components  $\nabla^2 \bar{v}_s = [\nabla^2 \bar{v}_{s,x}, \nabla^2 \bar{v}_{s,y}, \nabla^2 \bar{v}_{s,z}]$ , and  $\xi \bar{v}_s$ . As shown in de Groot-Hedlin (2008a), the first term yields an amplitude decrease proportional to the square of frequency and the second is a constant as a function of frequency. Thus, the equation for the particle velocity becomes

$$\rho_O \left( \frac{\partial \bar{v}_s}{\partial t} + \bar{v}_s \cdot \nabla \bar{v}_O + \bar{v}_O \cdot \nabla \bar{v}_s \right) + \rho_s \bar{v}_O \cdot \nabla \bar{v}_O = -\nabla p_s - \rho_s \bar{g} + \mu(\nabla^2 \bar{v}_s + \frac{1}{3} \nabla(\nabla \cdot \bar{v}_s)) + \xi \bar{v}_s + \bar{f} \quad (20)$$

Equations 20, 17, and 19 are a complete set of equations for propagation of infrasound energy, including attenuation, gravity, and wind, in a form amenable to FDTD implementation.

An example comparing infrasound propagation with and without attenuation through a model with constant sound speed and exponentially decreasing density (i.e., an isothermal atmosphere) is shown in Figure 3. Attenuation is

proportional to the square of the frequency and is equivalent to that at an altitude of 110 km. Pressure waveforms are sampled at locations shown above and below the source and are compared in Figure 4, along with associated waveforms.

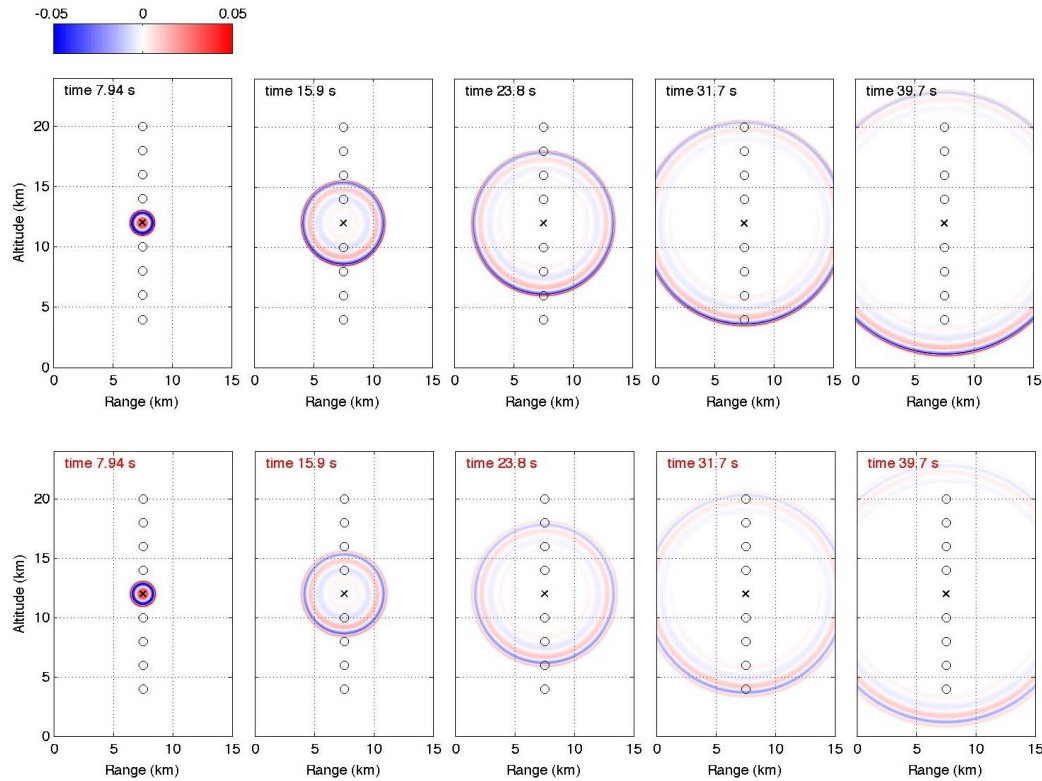


**Figure 3. (top) No attenuation. Waveforms are sampled at receiver locations shown by the circles. The source is indicated by an x. (bottom) same, but with attenuation equivalent to that at an altitude of 110 km.**

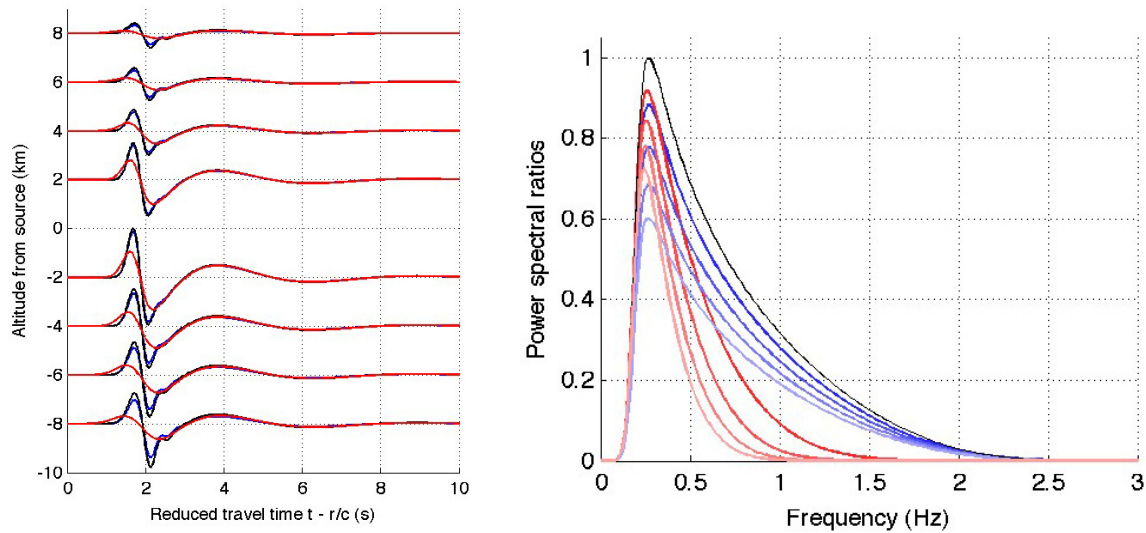


**Figure 4. (left) Waveforms are shown for no attenuation (black), constant attenuation (blue) and attenuation proportional to the square of the frequency (red, as shown in Figure 3b). (right) associated spectra, normalized with respect to peak power for waveforms propagated through non-attenuating media. Colored lines become lighter with increasing distance from the source.**

*Example of FDTD applied to penetration of infrasound into shadow zones*

Variations in wind velocities and temperature with altitude lead to the refraction of acoustic energy. During the day, temperatures and adiabatic sound speed typically decrease with altitude, causing sound to refract upward (Reynolds, 1873–1874). The effect of wind on refraction is often equal to or greater than that of temperature, so that sound is refracted downward in the direction of the wind and upward, away from the ground, in the opposite direction.

A first-order representation of acoustic “zones of silence” (ZoS) can be obtained using the high-frequency, ray-theory approximation as shown in Figure 5. Rays propagating through a moving atmosphere are computed using equations found in Garces (1998). Temperature decreases with altitude at a rate of  $6.5^{\circ}\text{C}/\text{km}$  (the environmental lapse rate) and the wind profile was chosen to approximately offset the associated decrease in sound speed with altitude. Rays were launched at an altitude of 2 km at a variable interval angle such that the ray endpoints would fall at 0.5 km increments on the surface for a homogeneous velocity model (to correct for cylindrical spreading at the surface). Therefore, the distance between ray endpoints in Figure 5 (or the ray density per unit length) is a measure of the pressure amplitude, and shows the degree of focusing and defocusing due to velocity heterogeneity. Pressure amplitude is slightly greater to the far right (in the wind direction). To the left, pressure amplitude quickly decreases starting at  $x = -5$  km and is effectively undetectable in the ZoS beginning at about  $x = -15$  km. In nature, the first ZoS away from a near-surface source typically extends from several kilometers from the source to between 120 and 200 km, depending on stratospheric winds.

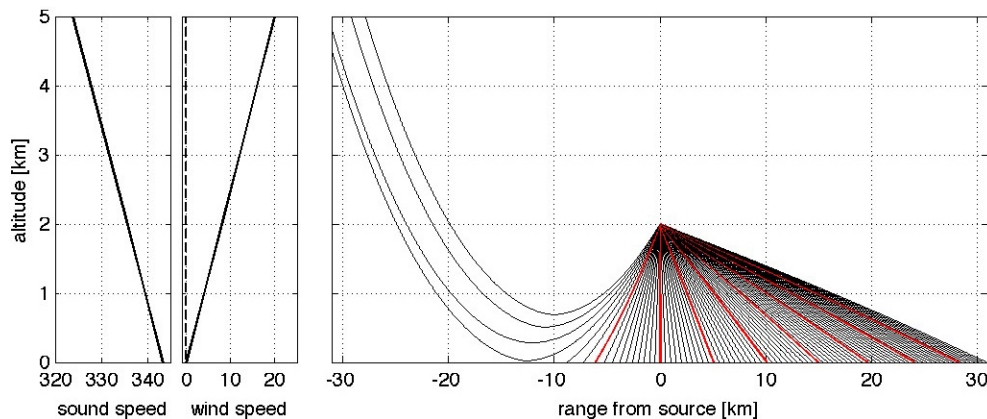


**Figure 5. A “zone of silence” (ZoS) illustrated by the high-frequency approximation of ray theory. The assumed adiabatic sound speed (m/s) and horizontal wind speed to the right (m/s) are shown in (a) and (b). The dashed line in (b) is out-of-plane wind speed (zero). Every tenth ray is red. Vertical exaggeration is 6.**

Ray theory relies on a high-frequency approximation to wave propagation. So its use assumes that sound speeds vary on a scale length much larger than the signal wavelength. This approximation starts to break down at infrasound frequencies under typical atmospheric conditions, where sound speed gradients of 4 m/s per km of altitude are common. A more complete description of infrasound propagation near the ground includes finite-wavelength effects like diffraction (Embleton, 1996), surface waves (Attenborough, 2002), scattering along rough topography, and also on temporal effects like turbulence and propagating gravity waves. These effects lead to a penetration of acoustic energy into the ZoS at amplitudes much greater than that predicted by ray theory (Embleton, 1996; Attenborough, 2002).

Zones of silence (ZoS) can be examined in better detail using numerical modeling algorithms that take dispersion, scattering, and other linear, full-wave effects into consideration. For instance, snapshots of the evolving pressure field are shown in Figure 6 from FD modeling using the same velocity model shown in Figure 5. The source (again at a 2-km altitude) consists of the superposition of a 0.9 Hz and a 0.2 Hz wavelet, multiplied by a cosine taper. Waveforms are shown at 5-km increments along the ground from -30 km to +30 km (Figure 7). The waveforms are scaled by the square root of the source-receiver distance to correct for spreading. Peak amplitudes are generally equal to the right, in agreement with the prediction from ray theory. However, the decrease in peak amplitude to the left is not as severe within the ZoS as predicted by ray theory. Lower frequencies are diffracted into the ZoS; the power spectra for each waveform show that 0.9 Hz energy decreases more rapidly than that around 0.2 Hz within the



ZoS. Therefore, ZoS predicted by ray theory may be completely penetrated by relatively lower-frequency infrasound, or exhibit frequency dependence with penetration distance. This is in line with observations: numerous studies have observed infrasound energy in classical shadow zones (e.g., Hedlin et al., 2008b; Ottemöller and Evers, 2008).

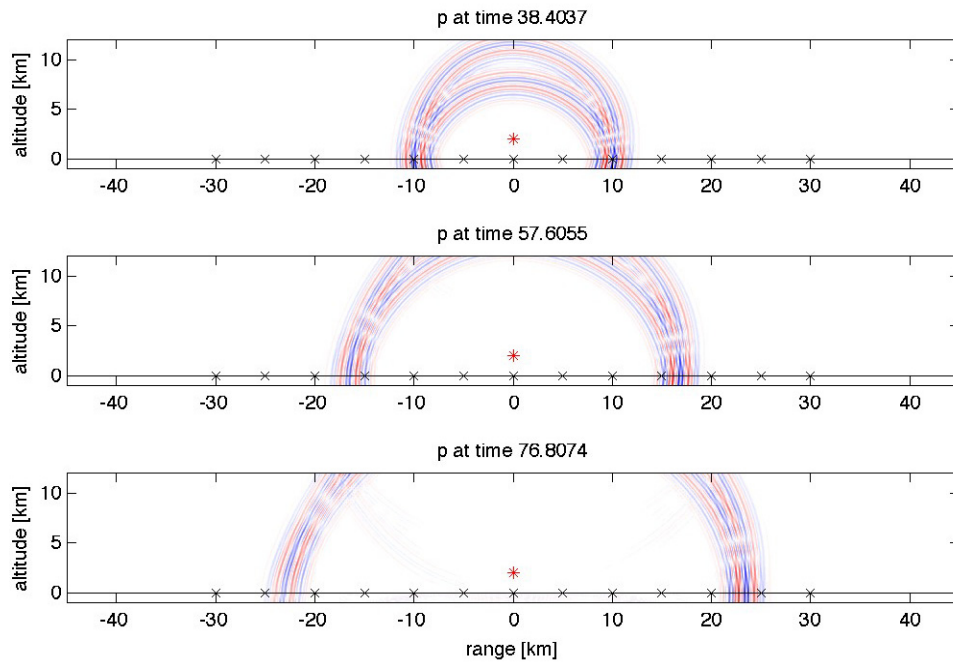


**Figure 6.** Pressure snapshots at 38.4, 57.6 and 76.8 seconds, derived from FD numerical modeling. The wind and sound speeds are the same as for Figure 4. The source is at 2 km in altitude, marked by a red asterisk, and receiver locations are marked by an x.

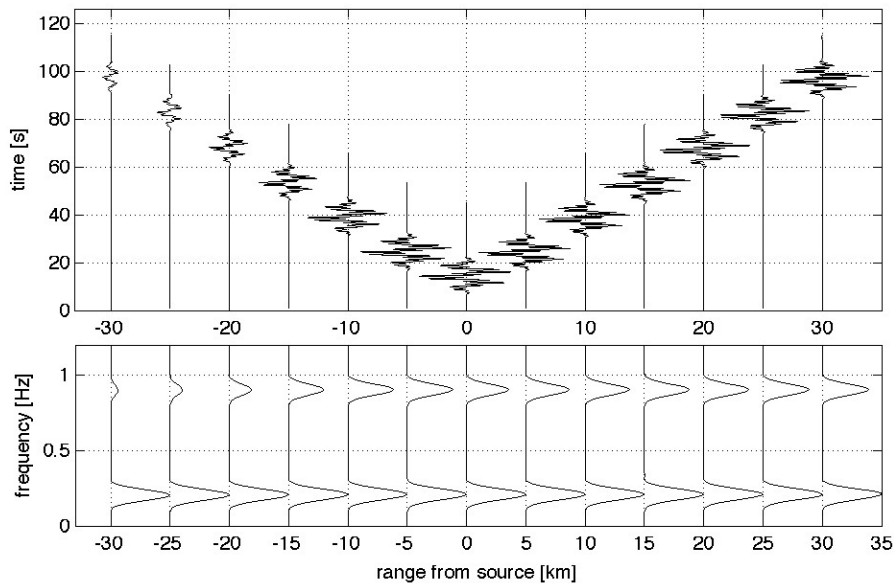


**Figure 7.** (top) Waveforms predicted from FD modeling for a source near a flat surface. Waveforms are corrected for spreading at receivers located at 5-km intervals along the ground. (bottom) Power spectra are normalized by the level of 0.2 Hz energy.

The FD algorithm was re-run, this time with variable topography to determine its effect on infrasound propagation into a shadow zone. The ground surface was modeled as a sine wave with a wavelength of 10 km, and a maximum height of 500 m. Receivers are located along the air/ground interface at an elevation of  $z=0$  m, since the receivers all lie along the zero crossings of the sine wave. Several snapshots are shown in Figure 8 and the waveforms and spectra are shown in Figure 9. As shown, the introduction of topography complicates the response. The waveforms are amplified at some point (e.g., at -10 km and at +15 km) and diminished at others (-15 km and +10 km and +20 km). The higher frequencies are diminished more than the low frequencies. The results suggest that ZoS depends not only on atmospheric temperatures (hence, adiabatic sound speed) and temperatures, but is also a complicated function of frequency and topography. The addition of topography appears to further strip off high frequencies in comparison to the case for flat topography (Figures 6 and 7 above).

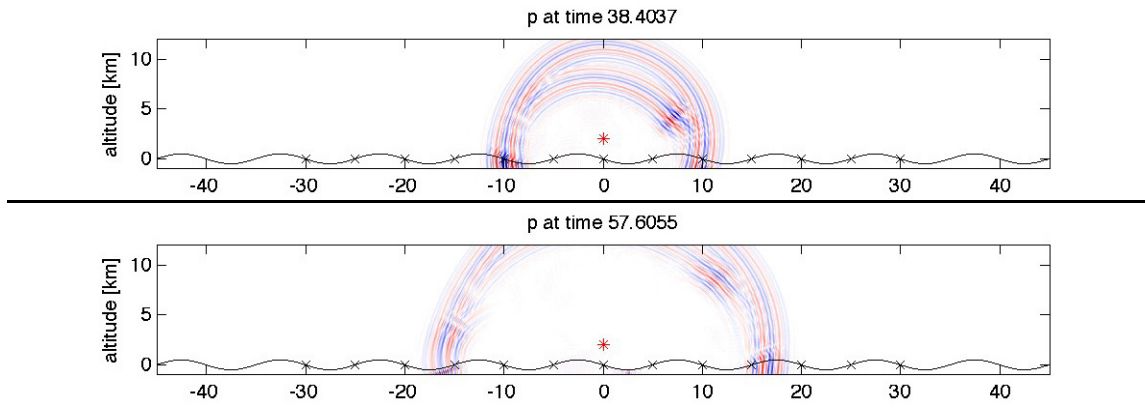


**Figure 8. Pressure snapshots at 38.4 and 57.6 seconds, derived from FD numerical modeling for the air/ground interface modeled as a sine wave. The wind and sound speeds are the same as for Figure 4. The source is at 2 km in altitude, marked by a red asterisk; receiver locations are marked by x. Receivers are at 0-km altitude, as in the previous example.**

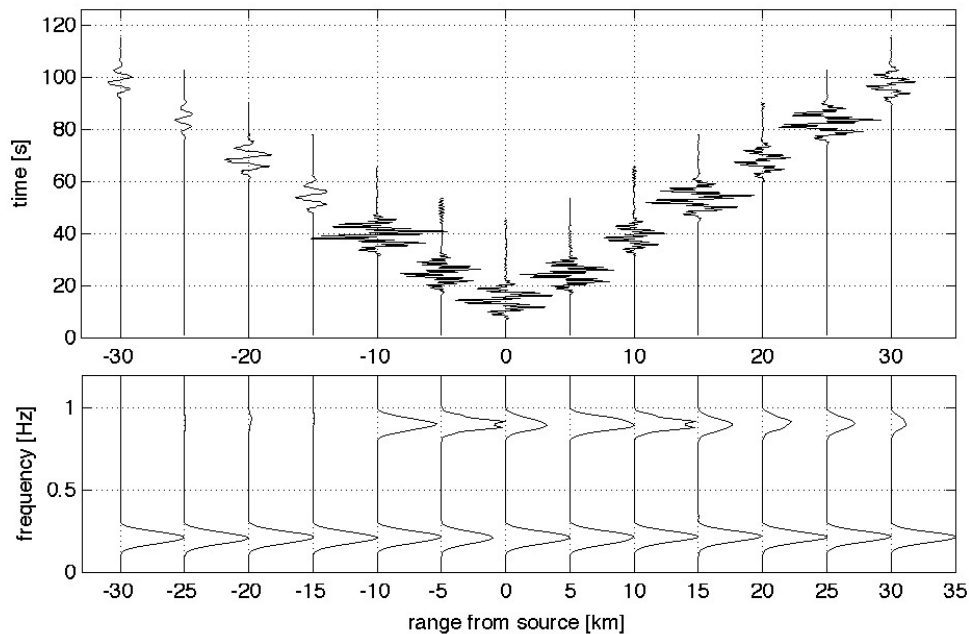


**Figure 9. (top) Waveforms predicted from FD modeling for a source near a sinusoidally varying surface. Waveforms are corrected for spreading at receivers spaced at 5-km intervals along the ground. (bottom) Power spectra are normalized by the level of 0.2 Hz energy.**

## **CONCLUSIONS AND RECOMMENDATIONS**

An algorithm has been developed to allow for the combined effects of wind and gravity on the infrasound field. The addition of attenuation into this code will be accomplished soon. The program is currently running slowly on a matlab platform. The plan is to convert it to fortran in the near future for considerable improvements in computational speed. After that, the code will be extended to three dimensions and tested against real data.

## **REFERENCES**

- Attenborough, K. (2002). Sound propagation close to the ground, *Annu. Rev. Fluid Mech.* 34: 51–82.
- Batchelor, G. K. (1967). *An introduction to fluid dynamics*, University Printing House, Cambridge.
- de Groot-Hedlin, C. (2008a). Finite difference time domain synthesis of infrasound propagation through an absorbing atmosphere, *J. Acoust. Soc. Am.*, [in press].
- de Groot Hedlin, C. D., Hedlin, M. A. H., Walker, K. T., Drob, D. P., and Zumberge, M. A. (2008b). Study of infrasound propagation from the Shuttle Atlantis using a large seismic network, *J. Acoust. Soc. Am.* [in press].
- Embleton, T. F. W. (1996). Tutorial on sound propagation outdoors, *J. Acoust. Soc. Am.* 100: 31–48.
- Garcés, M. A., R.A. Hansen, and K. G. Lindquist (1998). Travel times for infrasonic waves propagating in a stratified atmosphere, *Geop. J. Int.* 135: 255–263.
- Gill, A.E. (1982). *Atmosphere-Ocean Dynamics*, Academic Press, San Diego, CA.
- Hedin, A. E., Fleming, E. L., Manson, A. H., Schmidlin, F. J., Avery, S. K., Clark, R. R., Franke, S. J., Fraser, G. J., Tsuda, T., Vial, F., and Vincent, R. A. (1996). Empirical wind model for the upper, middle and lower atmosphere, *J. Atmos. and Solar-Terr. Phys.* 58: 1441–1447.
- Ostashev, V. E., D. K. Wilson, L. Liu, D. F. Aldridge, N. P. Symons, and D. Marlin (2005). Equations for finite-difference, time-domain simulation of sound propagation in moving inhomogeneous media and numerical implementation, *J. Acoust. Soc. Am.* 117: 503–517.
- Ottmöller, L. and L. G. Evers (2008). Seismo-acoustic analysis of the Buncefield oil depot explosion in the UK, 2005 December 11, *Geophys. J. Int.* 172: 1123–1134.
- Reynolds, O. (1873-1874). On the refraction of sound by the atmosphere, *Proc. Roy. Soc. London* 22: 531–548.
- Sutherland, L. C. and H. E. Bass (2004). Atmospheric absorption in the atmosphere up to 160 km, *J. Acoust. Soc. Am.* 115: 1012–1032.